COBEM 2023 27TH INTERNATIONAL CONGRESS OF MECHANICAL ENGENEERING

ABCM Brazilian Society of Mechanical Sciences and Engineering
27th ABCM International Congress of Mechanical Engineering
December 04-08, 2023, Florianópolis-SC, Brazil

COB-2023-2211
AERODYNAMIC VALIDATION OF VORTEX-BASED NON-LINEAR METHODS WITH LEADING-EDGE VORTEX SHEDDING

Tiago Priolli Monteiro
Instituto Tecnológico de Aeronáutica
tiagopmonteiro@yahoo.com.br

Kiran Ramesh
Hugh J. A. Bird
University of Glasgow
kiran.ramesh@glasgow.ac.uk, hja.bird@gmail.com

Flavio Silvestre
Technische Universität Berlin
flavio.silvestre@tu-berlin.de

Roberto Gil Annes da Silva
Instituto Tecnológico de Aeronáutica
gil@ita.br

Abstract. *The aerospace industry worldwide is seeking to develop "green aircraft" which are cleaner, quieter, and more efficient, based on demands for reduction of fuel burn, emission of pollutants and costs of operation. Aeroelastic behavior can impact these developments due to greater flexibility of lighter components, and non-linear aerodynamic models become necessary to simulate aeroelastic phenomena such as flutter. The LESP-modulated discrete vortex method introduces the Leading-Edge Suction Parameter (LESP) concept and presented an approach to allow for two-dimensional vortex-based methods to simulate the onset of leading-edge vortex (LEV) shedding and modulate its shedding during dynamic simulations. This concept was latter used to simulate limit-cycle oscillations on an airfoil at specific low-Reynolds number situations with good results. The same LESP concept was applied to the Unsteady Vortex-Lattice Method which allowed it to produce and modulate a LEV wake sheet in three-dimensional wings. This article aims to compare the two-dimensional and three-dimensional implementations of the LESP concept and study the three-dimensional effects that the UVLM expanded method produces when verified against LDVM and CFD for pitch-ramp-return motion of small and large aspect-ratio wing. The results show that the expanded UVLM produces very close results to LDVM for large aspect-ratios, where the wing tip effect is reduced, and was also capable of providing a good match for CFD results in small aspect-ratio wings. Therefore, both the two-dimensional and three-dimensional methods provide a good medium-fidelity method for low-Reynolds situations that can be applied to simulate flutter scenarios.*

Keywords: *Aerodynamics, Potential Flow, Leading-Edge Vortex, CFD*

1. INTRODUCTION

The aerospace industry worldwide is seeking to develop "green aircraft" which are cleaner, quieter and more efficient, based on demands for reduction of fuel burn, emission of pollutants and costs of operation. This has motivated studies into new aircraft designs and configurations by leading aircraft manufacturers such as Airbus, Boeing and Embraer. Most of these futuristic designs involve a higher level of structural flexibility than in conventional aircraft. Even currently, the trends in the aviation industry are to increase wing span (to reduce induced drag) and maximize use of composites (to reduce weight), which lead to increased structural flexibility. Flexible aircraft structures result in the aeroelastic behavior becoming closer in frequency to that of the flight dynamics. Current procedures for aeroelastic, flight mechanics, and flight control law design, which are based on decoupling between flight dynamics (rigid-body) and aeroelastic dynamics, may not be valid for flexible aircraft (Silvestre *et al.*, 2016).

Therefore, modeling flexible aircrafts introduces the challenge of coupling flight mechanics and aeroelasticity into the same framework. Murua *et al.* (2012) and Hesse and Palacios (2014) used a modal analysis structural formulation coupled with the Unsteady Vortex-Lattice Method to achieve medium-fidelity dynamic models that modeled aeroelasticity, with Silvestre and Luckner (2015) validating the modal approach coupled with an aerodynamic indicial solution for slightly flexible aircraft, where the amplitude of structural deformation is expected to remain small. Palacios *et al.* (2010)

tested several aerodynamic models, and concluded that the indicial method provided good results for high-aspect ratio wings when compared to UVLM, as long as the amplitudes remained low. As a result, these methods provided good results for scenarios that presented linear behavior for aerodynamic and structure dynamics.

However, a common concern in aeroelasticity that has major effects on aircraft flight dynamics is flutter. This phenomenon occurs when the combined damping from aerodynamics and structural rigidity becomes negative, and a self induced, oscillatory motion begins on the airframe. Owing to nonlinearities typically present in the aerodynamics and structure, the oscillatory motion may have a finite and limited amplitude, and this is characterized as a Limit-Cycle Oscillation (LCO). These oscillations may cause structural failure and hence it is important to be able to predict their occurrence and model their effects in various flight regimes.

Flutter has been modeled with linear analysis, using linear aerodynamic theories such as those by Theodorsen (Theodorsen, 1935) (Theodorsen and Garrick, 1942), in the frequency domain, and Wagner's indicial solution (Wagner, 1925), in the time domain. As LCOs are by their very nature nonlinear, these linear models are not capable of predicting all possible LCOs and their features. This inability to fully predict LCOs creates the need for extensive flight testing, which is an expensive and time-consuming endeavor. These problems are present all the more in highly flexible aircraft like High Altitude Long Endurance (HALE) or futuristic configurations and designs with large-aspect-ratio wings. In these aircraft, the aeroelastic behavior may be strongly influenced by the flight dynamics. A nonlinear aeroelastic analysis tool capable of predicting all aspects of LCO behavior is hence desirable (Denegri *et al.*, 2005).

A combined formulation of aeroelasticity and flight dynamics, using Computational Fluid Dynamics (CFD) for aerodynamics and Finite Element Method (FEM) for structural dynamics is an expensive problem, requiring several hours of computational time even with High Performance Computing (HPC) resources. Semi-empirical methods such as the Beddoes-Leishman (Leishman and Beddoes, 1989) or ONERA dynamic stall model (Petot, 1983) (Shearer and Cesnik, 2007) are typically used for inexpensive aeroelastic analysis in such regimes. These are computationally fast but do not provide insight into the flow phenomena and are only valid in regimes where they have been previously validated. Recognizing the need for a new class of low-cost and physics-based methods, low-order unsteady flow solvers based on phenomenological augmentataion of unsteady potential-flow methods, such as those by Ramesh *et al.* (2014) and Wang and Eldredge (2012) have been developed recently.

Tang *et al.* (2003) studied flutter and LCOs of 2D panels through linear theory and experiment, and noted that linear theory is unsuccessful in predicting the large-amplitude LCOs that occur owing to aerodynamic nonlinearities. Nonlinear aerodynamics resulting from viscous flow phenomena is largely dependent on the Reynolds number and the reduced frequencies involved, and leading-edge vortices (LEVs) have been seen to play a crucial role. In helicopter and wind-turbine applications that are characterised by large Reynolds numbers and low reduced frequencies, LEVs and the resulting dynamic stall phenomenon might lead to violent vibrations and mechanical failure (Leishman, 2002). Conversely, LEVs in high-frequency flows at low Reynolds numbers are responsible for the success of high-lift flight in insects (Ellington, 1995; Shyy and Liu, 2007; Ellington, 1999; Dickinson and Gotz, 1993), and high propulsive (Anderson *et al.*, 1998) and power-extraction (Kinsey and Dumas, 2008) efficiencies.

In this research, we are specifically concerned with aerodynamic non-linearities and analyzing the differences between a two-dimensional and three-dimensional LEV models for a prescribed moviment.

Ramesh *et al.* (2013) have developed time-stepping unsteady airfoil theory based on potential flow, which holds valid uniformly regardless of amplitude and reduced frequency of motion, and shape of trailing wake. This method was seen to predict aerodynamic forces well even under challenging conditions of large amplitude and high reduced frequency. To model flows with leading edge vortices(LEVs) (Eldredge and Jones, 2019), the Leading Edge Suction Parameter(LESP) was developed by Ramesh *et al.* (2011) to predict the onset of LEV formation. This parameter is a measure of the suction at the leading edge and it was shown that initiation of LEV formation always occurred at the same critical value of LESP, regardless of motion kinematics so long as the airfoil and Reynolds number of operation were the same. Using this criterion, a 2D discrete-vortex method was developed in which the LESP criterion was used to modulate the initiation, growth and termination of leading-edge vortices (Ramesh *et al.*, 2014). This method is abbreviated as LDVM (LESP-Modulated Discrete-Vortex Method), and has been successfully applied to study post-flutter limit-cycle oscillations of an airfoil (2D) constrained by torsional and translational springs (Ramesh *et al.*, 2015).

Ramesh *et al.* (2017) have applied the LDVM formulation to finite-wing (3D) flows using strip theory and a correction based on lifting-line theory and Yoshikazu *et al.* (2021) have attempted to adapt the LESP concept to Unsteady Vortex-Lattice Methods (UVLMs) for finite wings. Monteiro *et al.* (2020) investigated 3D aeroelastic models with a strip theory implementation of the LDVM model coupled with a modal-based structural model of a cantilevered wing, with the results indicating the capability of these low-order models to represent the LCOs characteristics with some limitations due to the 2D nature of the aerodynamic model. This work seeks to continue these investigations by verifying the differences between the two-dimensional LDVM and three-dimensional UVLM expanded with leading-edge vortex shedding when compared to CFD results in a pitch-ramp-return motion.

2. TWO-DIMENSIONAL LDVM MODEL

2.1 Nonlinear aerodynamic model (LDVM)

The LDVM aerodynamic model which is based on the 2D discrete-vortex method is used as the basis for the numerical modeling employed in this research. The model is extended to 3D using strip theory. This approximation is justified for the high-aspect-ratio wing considered in this research. The 2D LDVM method is first summarized below. The interested reader may refer to Refs. (Ramesh *et al.*, 2014, 2013) for further details.

2.1.1 Large-angle unsteady thin-airfoil theory

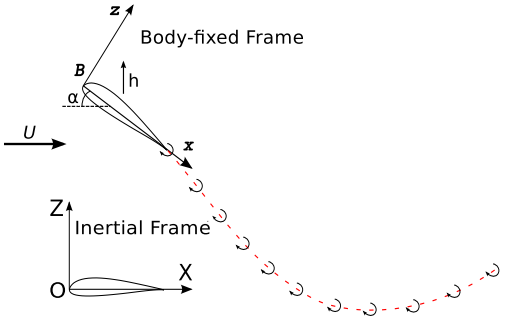

Figure 1. Depiction of time-stepping scheme.

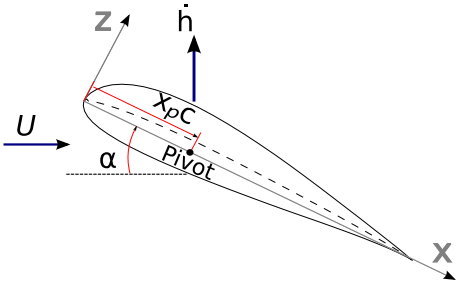

Figure 2. Airfoil velocities and pivot location.

At the foundation of the LDVM is a large-angle unsteady thin-airfoil theory detailed in Ramesh *et al.* (2013). This theory is based on the time-stepping formulation given by Katz and Plotkin (2000), but eliminates the traditional small-angle assumptions in thin-airfoil theory which may be invalid in flows of current interest. At each time step, a discrete vortex is shed from the airfoil trailing edge (referred to as TEV) as shown in figure 1. When dictated by the LESP-based shedding criterion (section 2.1.2), a discrete vortex is also shed from the leading edge at some time steps. The vorticity distribution over the airfoil at any given time step is taken to be a Fourier series truncated to r terms:

$$\gamma(\theta) = 2U\left[A_0\frac{1+\cos\theta}{\sin\theta} + \sum_{i=1}^{r} A_i \sin(i\theta)\right] \tag{1}$$

where the transformation variable θ relates to the chordwise coordinate as: $x = c(1-\cos\theta)/2$, with x measured from the leading edge; that is, $0 \le x \le c$ and $0 \le \theta \le \pi$. A_0, A_1, ..., A_r are the time-dependent Fourier coefficients, and U is the freestream velocity. The Kutta condition (zero vorticity at the trailing-edge) is enforced implicitly through the form of the Fourier series. The Fourier coefficients are calculated by enforcing the boundary condition of zero normal flow through the airfoil camberline as

$$A_0 = -\frac{1}{\pi}\int_0^{\pi}\frac{W(\theta)}{U}d\theta, \tag{2}$$

$$A_i = \frac{2}{\pi}\int_0^{\pi}\frac{W(\theta)}{U}\cos(i\theta)d\theta, \tag{3}$$

where $W(\theta)$ is the induced velocity normal to the airfoil camberline. This value is calculated from components of motion kinematics, depicted in figure 2, and induced velocities from all vortices in the flowfield.

When there is no LEV shedding in a time step, the only unknown is the strength of the last-shed trailing-edge vortex and this is calculated iteratively such that Kelvin's circulation condition is satisfied (Ramesh *et al.*, 2013).

2.1.2 LESP criterion for LEV formation and shedding

The LESP is a measure of the suction peak at the leading edge, which in turn is caused by the stagnation point moving away from the leading edge when the airfoil is at an angle of attack. From Garrick (1937) and von Kármán and Burgers (1963), the suction at the leading edge in potential flow may be expressed as

$$S = \lim_{x \to LE} \frac{1}{2}\gamma(x)\sqrt{x}. \tag{4}$$

Evaluating using the current formulation, $S = \sqrt{c}UA_0$. The Leading Edge Suction Parameter is defined as a nondimensional value of suction at the leading edge, and is hence simply set equal to the first coefficient from Eq. (1), A_0.

Katz (1981) has noted that real airfoils have rounded leading edges which can support some suction even when the stagnation point is away from the airfoil leading edge. The amount of suction that can be supported depends on the airfoil shape and Reynolds number of operation. When these quantities are kept constant, it was shown in Ramesh *et al.* (2014) that initiation of LEV formation always occurred at the same value of LESP regardless of motion kinematics and history. This threshold value of LESP, which is a function of the airfoil shape and Reynolds number, is termed the critical LESP. This value, for any given airfoil and Reynolds number (and other specific operating conditions such as freestream turbulence and the presence of roughness), can be obtained from CFD or experimental predictions for a single motion (Ramesh *et al.*, 2014), and can then be used for any other motion to predict LEV formation. In the LDVM model, a discrete vortex is shed is from the leading edge at those time steps when the instantaneous LESP (A_0 value) is greater than the critical LESP value. The strength of the LEV is determined such that the instantaneous LESP value, which would have otherwise exceeded the critical LESP value, is made equal to the latter. This condition, along with Kelvin's condition, is used to determine shed vortex strengths iteratively in time steps where both TEV and LEV are shed.

2.1.3 Vortex method details and Implementation

In the current approach, the vortex-core model proposed by Vatistas *et al.* (1991), which approximates the Lamb-Oseen vortex is used to model the discrete vortices as vortex blobs. In this model, the velocities induced at X and Z (u and w) by the k^{th} vortex in the X and Z direction are:

$$[u, w] = \frac{\gamma_k}{2\pi} \frac{[(Z - Z_k), (X_k - X)]}{\sqrt{\left[(X - X_k)^2 + (Z - Z_k)^2\right]^2 + v_{core}^4}}. \tag{5}$$

where X_k and Z_k are the positions of the k^{th} vortex. The vortex core radius, v_{core}, in the simulations was set as $0.02c$, where c is the section chord. To control vortex count and limit the computational cost, vortices that are a distance greater than ten chord lengths from the airfoil are deleted. A fixed nondimensional time step (dt^*) of 0.015 was used to advance the solution in time. Further details about the choice of these parameters may be found in Ramesh *et al.* (2014) and Ramesh *et al.* (2015). The dimensional time step is calculated as $dt = dt^* \frac{c}{U}$.

In recent work, SureshBabu *et al.* (2019) and Darakananda *et al.* (2018) have developed model-reduction methods for discrete-vortex methods where amalgamation of vortex blobs is implemented to drastically reduce the vortex count and speed up the code. In the current research, such model reduction methods were not used.

2.1.4 Force and Moment Calculation

Once the vorticity distribution on the airfoil is determined, the normal (c_n) and suction (c_s) coefficients are calculated by equations 6 and 7 respectively.

$$\begin{aligned} c_n = \frac{Fn}{q_\infty c} = 2\pi[\frac{(U\cos\alpha + \dot{h}\sin\alpha)}{U}(A_0 + \frac{1}{2}A_1) + \\ + \frac{3c}{4U}\dot{A}_0 + \frac{1c}{4U}\dot{A}_1 + \frac{1c}{8U}\dot{A}_2 + \frac{2}{U^2 c}\sum_{n=1}^{ndiv}(\frac{\partial\phi_{lev_n}}{\partial x} + \frac{\partial\phi_{tev_n}}{\partial x})\gamma(x,t) \end{aligned} \tag{6}$$

$$c_s = \frac{F_s}{q_\infty c} = 2\pi A_0^2 \tag{7}$$

Where, ϕ_{lev_n} and ϕ_{tev_n} are the velocity potential from leading edge vortices and trailing edge vortices respectively.

The lift coefficient is calculated by combining Normal and Suction coefficients (equation 8) and the moment coefficient, c_m is calculated by dividing the moment around the pivot (m_{ea} given by equation 9, where $x_{ea} = X_p c$ and X_p is the pivot position as a fraction of the chord) by $\frac{1}{2}\rho U^2 c^2$.

$$c_l = c_n\cos(\alpha) + cs\sin(\alpha) \tag{8}$$

$$m_{ea} = x_{ea}F_N - \rho\pi c^2 U[(U\cos(\alpha) + \dot{h}\sin(\alpha))(\frac{1}{4}A_0 + \frac{1}{4}A_1 - \frac{1}{8}A_2) + \\ + c(\frac{7}{16}\dot{A}_0 + \frac{11}{64}\dot{A}_1 + \frac{1}{16}\dot{A}_2 - \frac{1}{64}\dot{A}_3)] - \rho\sum_{n=1}^{ndiv}(\frac{\partial\phi_{lev_n}}{\partial x} + \frac{\partial\phi_{tev_n}}{\partial x})\gamma(x,t)x \tag{9}$$

3. THREE-DIMENSIONAL UVLM MODEL

The Unsteady Vortex-Lattice Method (UVLM) is a time-stepping aerodynamic solution for a three-dimensional wing. The method is implemented for a defined wing movement and allows the calculation of force and moment coefficients with relative precision. The implementation used for base UVLM method (without LEV shedding) is based on the work of Katz and Plotkin (2000). The method discretizes the wing into panel elements, at each panel a vortex ring is positioned with the lead line at the quarter chord position and collocation points at the three-quarter panel position 3.

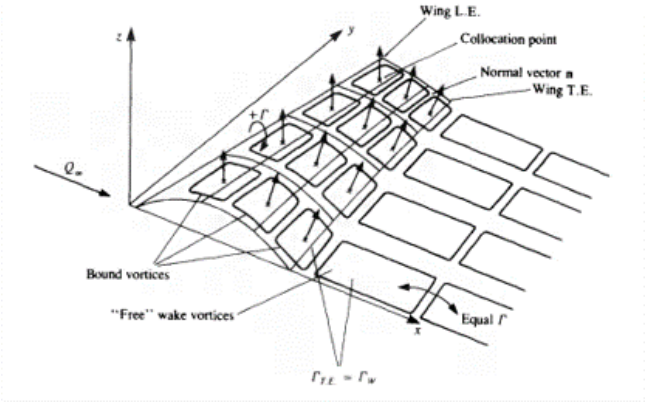

Figure 3. UVLM concept image Katz and Plotkin (2000)

The core of the model consists in applying the Kelvin condition and defining the flow at the collocation points to be parallel to the wing surface. To that effect equation 10 is calculated at each time-step. Solving this equation results in the circulation of each panel that is bounded to the wing. The influence coefficient matrix represents the influence of each bounded panel in the other panels (equation 12), whereas the RHS vector represents the downwash at each collocation point resulted from the motion kinematics and wake influence (equation 13). The wake rings have a fixed circulation after they are shed and can flow freely with the velocity stream. Finally, by positioning the vortex ring main line in the quarter-chord of each panel the kelvin and kutta condition are automatically fulfilled, with the wake being shed at the trailing edge.

$$\begin{pmatrix} a_{11} & a_{12} & \cdots & a_{1m} \\ a_{21} & a_{22} & \cdots & a_{2m} \\ \vdots & \vdots & \ddots & \vdots \\ a_{m1} & a_{m2} & \cdots & a_{mm} \end{pmatrix} \begin{pmatrix} \Gamma_1 \\ \Gamma_2 \\ \vdots \\ \Gamma_m \end{pmatrix} = \begin{pmatrix} RHS_1 \\ RHS_2 \\ \vdots \\ RHS_m \end{pmatrix} \tag{10}$$

Where,

$$m = M_{panelRows} * N_{panelCollumns} \tag{11}$$

$$a_{kl} = \begin{pmatrix} u \\ v \\ w \end{pmatrix}_{induced} \cdot n_k \tag{12}$$

$$RHS_k = \left(\begin{pmatrix} u_i \\ v_i \\ w_i \end{pmatrix}_{wake} + \begin{pmatrix} u(t) \\ v(t) \\ w(t) \end{pmatrix}_{kinematics} \right) \cdot n_k \tag{13}$$

Solving this system of equation results in the vortex strengths bound to the wing. They are the basis for calculating the pressure difference between upper and lower wing surfaces. For each panel in the discrete wing the pressure difference between upper and lower surfaces is calculated by equation 14, with the force acting on that panel defined by equation 15.

$$\begin{aligned}\Delta p_{ij} = \rho([U(t)+u_W, V(t)+v_W, W(t)+w_W]_{ij} \cdot \tau_i \frac{\Gamma_{i,j}-\Gamma_{i-1,j}}{\Delta c_{ij}} \\ +[U(t)+u_W, V(t)+v_W, W(t)+w_W]_{ij} \cdot \tau_j \frac{\Gamma_{i,j}-\Gamma_{i,j-1}}{\Delta b_{ij}} + \frac{\delta}{\delta t}\Gamma_{ij})\end{aligned} \tag{14}$$

$$\Delta \mathbf{F}_{ij} = \Delta p_{ij} \Delta S_{ij} \mathbf{n}_i j \tag{15}$$

Where $[U(t), V(t), W(t)]$ is the kinematic contribution, $[u_W, v_W, w_W]$ is the wake contribution, τ_i and τ_j are the tangent unit vector chordwise and spanwise, respectively. Δc_{ij} and Δb_{ij} are the panel sizes, chordwise and spanwise respectively. Finally, ρ is the air density, ΔS_{ij} is the panel area and $\mathbf{n}_{ij}$ is the normal vector at the panel. Lift and Moment coefficients were calculated for each spanwise location by combining the forces and moments of every chordwise panel. Equations 16 and 17 show how the lift and moment coefficient calculation for each spanwise location.

$$C_{Lj} = \frac{\sum \Delta F(3)_{ij}}{q_\infty S_1} \tag{16}$$

$$C_{Mj} = \frac{\sum L * (x_j^{pvt} - x_{ij}^{\Gamma})}{q_\infty c S_1} \tag{17}$$

Where the x_j^{pvt} is the aerodynamic pivot position for the spanwise position j, x_{ij}^{Γ} is the vortex ring position at the panel, and q_∞ is the dynamic pressure.

For the wake rollup a simple first degree discrete equation was applied (Equation 18). This equation calculates the induced velocity at each vertice produced by all wake and bound panels. The velocity is multiplied by the time-step to get the displacement. Yoshikazu (2016) performed many verifications with more complex models, however it was noticed that higher order methods do little to improve wake rollup accuracy and therefore for this article the simpler first-order method was used. The chart below (figure 4) presents a visual representation of the model execution engine.

$$\begin{pmatrix} X_{TEV} \\ Y_{TEV} \\ Z_{TEV} \end{pmatrix}_t = \begin{pmatrix} X_{TEV} \\ Y_{TEV} \\ Z_{TEV} \end{pmatrix}_{t-1} + \left(\begin{pmatrix} U_i \\ V_i \\ W_i \end{pmatrix} + \begin{pmatrix} U_{iTEV} \\ V_{iTEV} \\ W_{iTEV} \end{pmatrix} \right) * dt \tag{18}$$

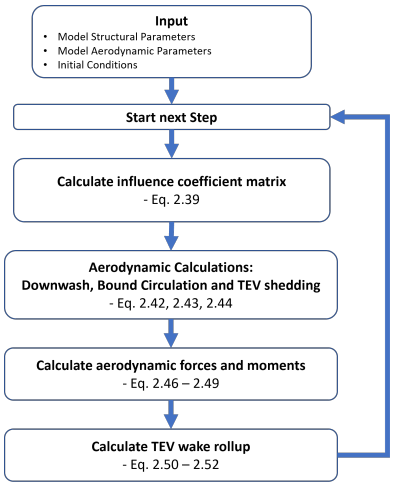

Figure 4. UVLM execution chart

3.1 Expanding UVLM with Leading-Edge Vortex Shedding

In order to add Leading-edge vortex shedding to UVLM a few changes need to be performed to the overall model execution engine. Basically, the process is edited after the bound circulation is calculated. Aggarwal (2013) proposes that in the region near the leading edge, the forwardmost vortex lattice circulation can be directly represented by the A_0 term from the Fourier series. Since, in LDVM, LESP derivates directly from the A_0 he proposes a formulation that does not depend heavily on the number of chordwise panels and provides a effective way to calculate A_0 at each spanwise location. Equation 19 provides this result. Aggarwal also proposes that this formulation is adjusted by a 13% factor to better match the LDVM results.

$$LESP(y) = \frac{\Gamma_1(y)}{U_{\inf} c[cos^{-1}(1-(2\Delta x_l/c)) + sin(cos^{-1}(1-(2\Delta x_l/c)))]} \tag{19}$$

If $LESP$ is greater than $LESP_{crit}$ than a LEV will be shed at a that spanwise location. The LEV is positioned depending on the history for the particular location.

The first LEV shed a given location is located at:

$$x_L = v_{ind}\Delta t \tag{20}$$

Where v_{ind} is the induced velocity at the leading edge. However if LEVs were shed in the previous step at the same location, than the new panel is located at:

$$x_{L,n} = \frac{2}{3}x_{i,L.E.} + \frac{1}{3}x_{L,n-1} \tag{21}$$

The circulation for the new LEV is defined by a Newton-Raphson optimization that seeks to equate $LESP$ and $LESP_{crit}$. Equation 22 is executed inside a loop until this definition is met.

$$\Gamma_L^k = \frac{\Gamma_L^{k-1} - \Gamma_L^{k-2}}{LESP^{k-1} - LESP^{k-2}}(LESP_{crit} - LESP^{k-1}) + \Gamma_L^{k-1} \tag{22}$$

Yoshikazu (2016) proposed that a pseudovortex was added to the strips that are shedding LEV. Since the LEV sheet starts at the geometric leading edge of the wing, and forwardmost bound vortex only starts at the quarter position of the panel, a circulation disconnect from the flow would appear at the leading edge. Therefore the pseudo-vortex was added with strenght equal to the currently shed LEV that connects the LEV wake to the rest of the vortices in he UVLM model and was initially proposed to connect the LEV sheet to the TEV wake sheet, as shown in figure 5. For this article a simple change was performed to connect the LEV sheet to the bound voltices instead of the TEV wake. This option was favored because it kept the UVLM model closer to its original form, with no changes needed to be made to the TEV shedding circulation. Therefore, a pseudo vortex with strength equal to the LEV with opposite signal connecting the LEV vortex to the first bound vortex was added to the model impacting the downwash calculation and the changing equation 19 to 23.

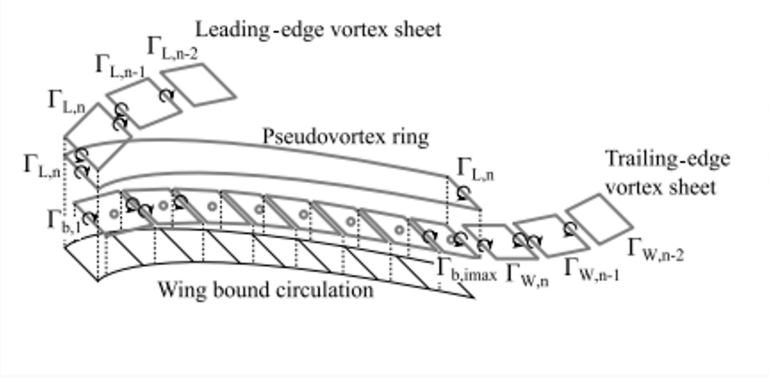

Figure 5. Pseudovortex ring ((Yoshikazu *et al.*, 2021))

$$LESP(y) = \frac{\Gamma_1(y) - \Gamma_{LEV}(y)}{U_{\inf} c[cos^{-1}(1-(2\Delta x_l/c)) + sin(cos^{-1}(1-(2\Delta x_l/c)))]} \tag{23}$$

With LEV and bound circulation now adhering to the Kelvin condition where $LESP = LESP_{crit}$, the UVLM can proceed with forces and moments calculation. Figure 6 shows in red the main additions that are made to UVLM to allow for LEV shedding. Finally, it is important to notice that one of the sources of instability in LEV enhanced UVLM models is the LEV wake rollup. Specially when the LEV sheet interacts with the wing bounded vortex rings, the velocity field at the wake's vertices can get close to a singularity point when it crosses a cortex segment. To reduce this effect, Hirato proposed a region close the surface of the wing where teh velocity field is considered only in the direction parallel to the surface, disregarding any normal velocity field effects produced at this region (Yoshikazu, 2016). For this implementation is region is considered from the second chord-wise ring to the second-last chord-wise ring.

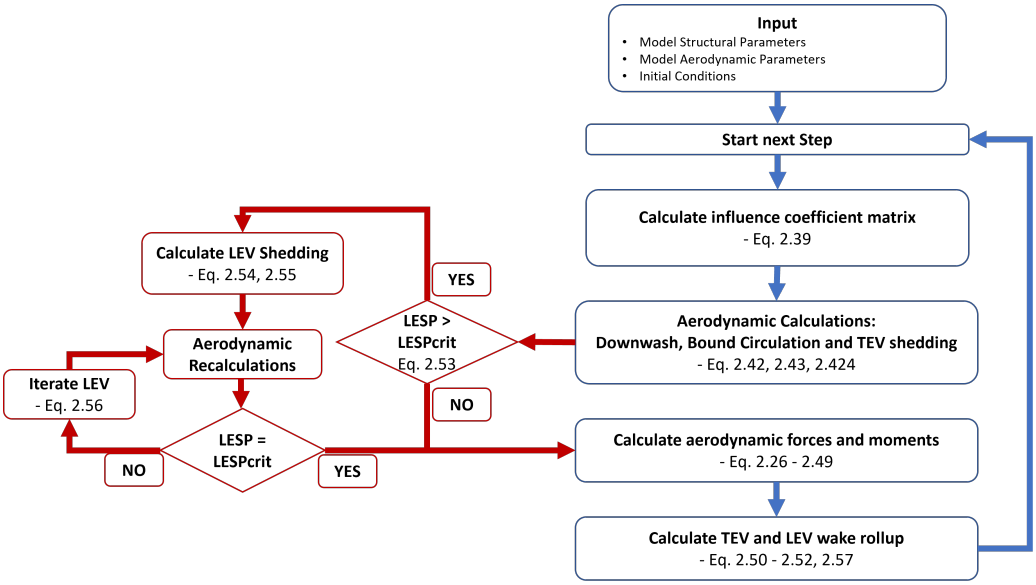

Figure 6. UVLM with LEV execution chart

4. COMPUTATIONAL FLUID DYNAMICS FORMULATION

To provide a basis for comparison between two-dimensional and three-dimensional methods, CFD results of pitch-ramp-return scenario was used. The CFD results used in this article are based on the experiments conducted by Bird and Ramesh (2022). The CFD results were executed using the open-source CFD toolbox OpenFOAM. For low-Reynolds-number case studied, a body-fitted, structured computational mesh is moved according to prescribed pitch kinematics, and the time-dependent governing equations are solved using a finite volume method. A second-order backward implicit scheme is used to discretize the time derivatives, and second-order limited Gaussian integration schemes are used for the gradient, divergence and Laplacian terms. Pressure-velocity coupling is achieved using the pressure implicit with splitting of operators (PISO) algorithm. The $Re = 10000$ cases were computed following the experimentally-validated RANS method used in Bird *et al.* (2021), albeit with different kinematics. The Spalart-Allmaras (SA) turbulence model (Spalart and Allmaras, 1992) is used for turbulence closure, with the trip terms in the original SA model turned off. For the low Reynolds number cases considered in this research, the effects of the turbulence model are confined to the shed vortical structures and wake. The meshes are the same as those used in Bird *et al.* (2021). In this paper, a rectangular wing of chord length $c = 0.1$m and aspect ratio of 3 is considered. An $O - mesh$ topology was used with 116 cells in the chordwise direction. The mesh was finer near the leading and trailing edges. Since the pitch kinematics are symmetrical about the wing center, only half the wing was meshed. The aspect ratio 3 half-wing meshes had 105 cells in the spanwise direction. The spanwise domain extends 4 chord lengths beyond the wingtip with an average spacing of 21 cells per chord length in this region. In the wall-normal direction, cell spacing begins at $1.5\text{x}10^{-5}$m next to the wall $(\gamma+ < 1)$ and extends a distance of 11.5 chord lengths away from the wing with an average density of 16.3 cells per chord length. The simulations were carried out at a free stream velocity $U_1 = 0.1$m/s and kinematic viscosity $10^{-6}\text{m}^2/\text{s}$ to obtain a chord-based Reynolds number of 10000.

The table 1 below summarizes the parameters used for the UVLM and LDVM model.

5. RESULTS AND DISCUSSION

In order to validate the UVLM expanded model and verify its characteristics the following tests were performed (table 2).

In order to better assess the capabilities of the extended UVLM implementation it was first verified against a pure

Chord (m)	0.10
Span (m)	0.30
Freestream velocity (m/s)	0.1
Air density (kg/m^3)	1.225
UVLM Number of panels in spanwise direction	60
UVLM Number of panels in chorwise direction	20
LDVM Number of chordwise vortices	70
LDVM Number of fourier terms	35
Pivot position as a fraction of the chord (0-1)	0
Reference Reynolds number	10000
Critical LESP	0.30
Non-Dimensional time step	0.015

Table 1. Model Parameters

Test Number	Test Description
01	Numerical validation of LESP Calculation in UVLM vs LDVM
02	Forces and moments verification against CFD results
03	LEV wake development over time

Table 2. Tests performed

LDVM model in its capacity to correctly calculate the Leading-edge suction parameter. Figure 7 shows the effects of the aspect-ratio in the results produced by UVLM and how it relates to the 2D results form LDVM. On the left of figure 7 it is possible to verify that with an increase in aspect ratio, wing tip effects become less relevant and the UVLM lift coefficient approximate LDVM. It is also possible to get a sense of the effect that suction force has on the overall lift coefficient when the LESP calculation is corrected with the 13% increase proposed by Aggarwal (2013). On the right side of figure 7 the LESP value is directly compared displaying the effect that wing tip effects have on the LESP result, as well as the effect that the correction has on LESP behavior.

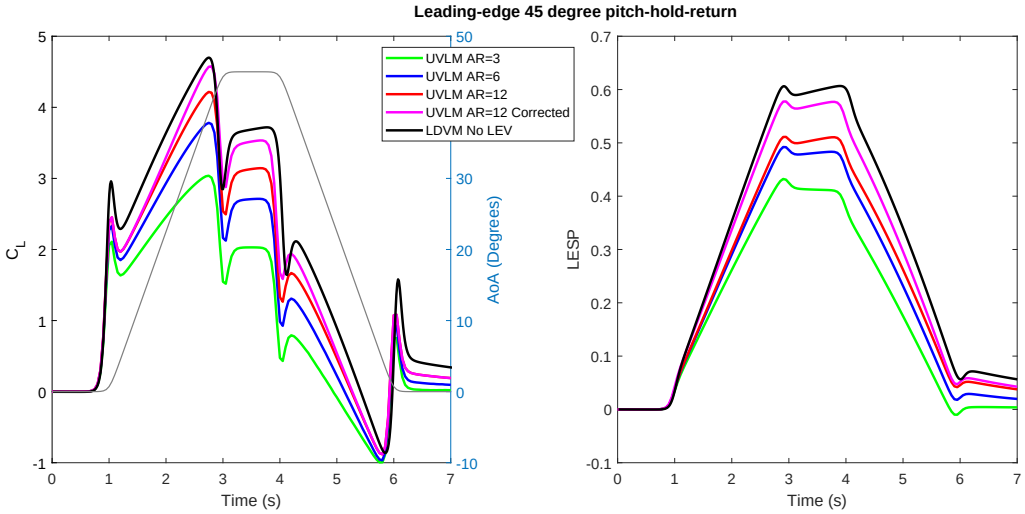

Figure 7. LESP Validation

For the second verification, CFD results were added to compare the lift results between extended UVLM, base UVLM and the LDVM counterparts (both with and without LEV shedding). Figure 8 shows the C_L comparison between models with LEV shedding and without. It is possible to verify that LDVM overestimates the forces due to the wing tip effects that are significant in the small aspect-ratio of AR3 analyzed. LEV shedding on the LDVM reduces the C_L produced at the wing at the pitch ramp portion of the curve and keeps this influence as long as the there are leading-egde vortices above the wing. UVLM full three-dimensional modeling approximates the CFD results very well for the pitch-up motion. The effect of LEV wake sheet seems to mirror that from the LDVM model, with a slight reduction on the C_L during the pitch up and hold motions, however during pitch-down the effect of the LEV sheet increases the C_L.

It is only by analyzing the LEV wake development more closely that it is possible to fully understand the results from the UVLM model. Figures 9 and 10 show the LEV formation at time equals 4s for UVLM and LDVM respectively. At this

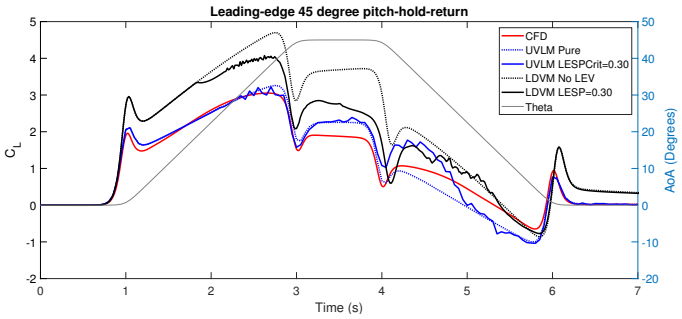

Figure 8. LEV Shedding Simulation

point the wing is is at the end of the hold motion. A roughness in LEV sheet is apparent and the wake roll is perceptible as it begins to move over the trailing edge of the wing. The LDVM model present a similar formation with the LEV vortices starting to move to the trailing-edge of the airfoil. The roughness observed in UVLM is the main cause for the peaks that appear in the UVLM result with LEV, and is a direct result from the high velocities produced by the singularity points at the vortex segments that compose the rings bounded to the wing. Yoshikazu *et al.* (2021) notices in his thesis that, even with the correction applied to the center of the wing, this effect can happen, and used an amalgamation routine to smooth out this behavior and produce a more stable result. At time 5s (figure 11) the LEV shedding has stopped as the wing is half-way to return to the initial position, the LEV sheet is mostly out of the wing and this causes the forces to get closer to the base UVLM model. At the same time the LDVM model also has stopped shedding LEV and the LEVs are rolling out of the airfoil surface (figure 12).

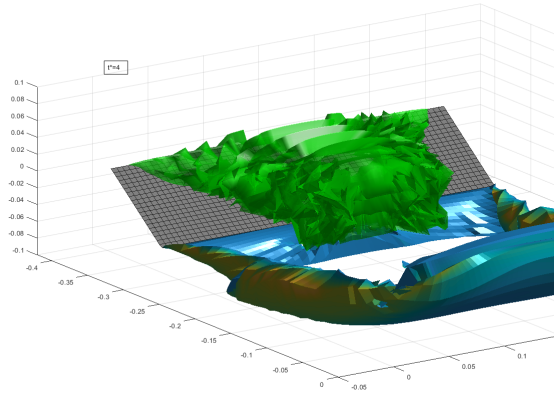

Figure 9. UVLM Vortex (t=4s)

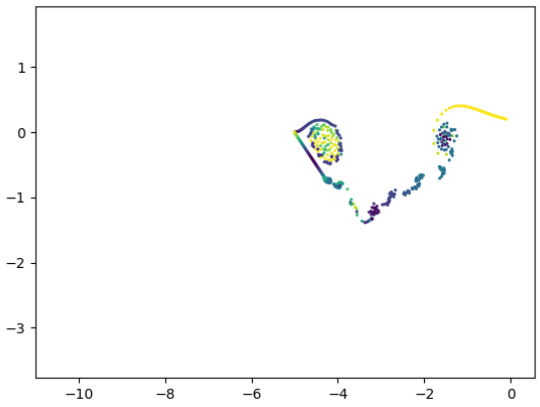

Figure 10. LDVM Vortex (t=4s)

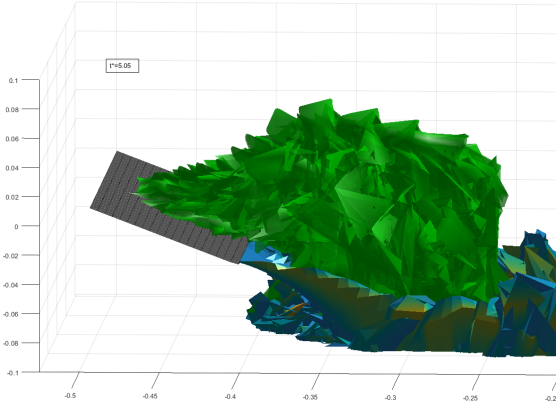

Figure 11. UVLM Vortex (t=5s)

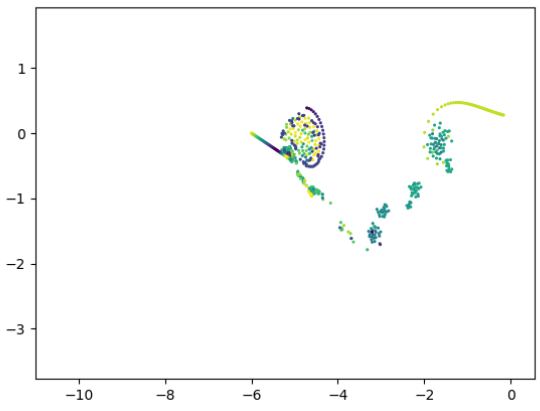

Figure 12. LDVM Vortex (t=5s)

6. CONCLUSIONS

The results presented in this article show that using LESP-Modulated models offers a good trade-off between generating non-linear aerodynamic results and faster computational time. The 2D and 3D models can be setup to predict the onset of LEV shedding and provide good behavior approximation, specially for the the pitch-up movement. For high aspect-ratio wings both the 2D and 3D models should provide acceptable results, however, on low aspect-ratio wings the wing tip effects become too strong and a three dimensional wing modeling is better suited for generating the results.

The results can be further improved by applying some advanced techniques such as ring amalgamation to reduce roughness observed at the LEV wake sheet. For future works, the authors intend to apply the three-dimensional model to a aeroelastic wing model and simulate LEV induced limit-cycle oscillations after the linear flutter point.

7. ACKNOWLEDGEMENTS

This study was financed in part by the Coordenação de Aperfeiçoamento de Pessoal de Nível Superior – Brasil (CAPES) – Finance Code 001

8. REFERENCES

Aggarwal, S., 2013. *An inviscid numerical method for unsteady flows over airfoils and wings to predict the onset of leading edge vortex formation*. Master's thesis, North Carolina State Universit.

Anderson, J., Streitlien, K., Barrett, D. and et al, 1998. "Oscillating foils of high propulsive efficiency". *Journal of Fluid Mechanics*, Vol. 360(1).

Bird, H.J.A. and Ramesh, K., 2022. "Applying frequency-domain unsteady lifting-line theory to time-domain problems". *AIAA Journal*.

Bird, H.J.A., Ramesh, K., Otomo, S. and Viola, I.M., 2021. "Applying inviscid linear unsteady lifting-line theory to viscous large-amplitude problems". *AIAA Journal*.

Darakananda, D., Silva, A.F.C., Colonius, T. and Eldredge, J.D., 2018. "Data-assimilated low-order vortex modeling of separated flows". *Physical Review Fluids*.

Denegri, C.M., Dubben, J.A. and Maxwell, D.L., 2005. "In-flight wing deformation characteristics during limit cycle oscillations". *Journal of Aircraft*, Vol. 42(2).

Dickinson, M.H. and Gotz, K.G., 1993. "Unsteady aerodynamic performance of model wings at low reynolds numbers". *Journal of Experimental Biology*, Vol. 174(1).

Eldredge, J.D. and Jones, A.R., 2019. "Leading-edge vortices: Mechanics and modeling". *Annual Review of Fluid Mechanics*.

Ellington, C.P., 1995. "Unsteady aerodynamics of insect flight". *Symposia of the Society for Experimental Biology*, Vol. 49.

Ellington, C.P., 1999. "The novel aerodynamics of insect flight: applications to micro-air vehicles". *Journal of Experimental Biology*, Vol. 202(23).

Garrick, I.E., 1937. "Propulsion of a flapping and oscillating airfoil". NACA Rept. 567.

Hesse, H. and Palacios, R., 2014. "Reduced-order aeroelastic models for dynamics of maneuvering flexible aircraft". *AIAA Journal*.

Katz, J., 1981. "Discrete vortex method for the non-steady separated flow over an airfoil". *Journal of Fluid Mechanics*, Vol. 102(1).

Katz, J. and Plotkin, A., 2000. *Low-Speed Aerodynamics*. Cambridge Aerospace Series.

Kinsey, T. and Dumas, G., 2008. "Parametric study of an oscillating airfoil in a power-extraction regime". *AIAA Journal*, Vol. 46(6).

Leishman, J.G., 2002. "Principles of helicopter aerodynamics". *Cambridge Aerospace Series*.

Leishman, J.G. and Beddoes, T.S., 1989. "A semi-empirical model for dynamic stall". *Journal of the American Helicopter Society*, Vol. 34(3).

Monteiro, T.P., Ramesh, K., Silvestre, F. and Silva, R.G.A., 2020. "Coupled framework for limit-cycle oscillations modeling based on leading-edge vortex shedding". *Journal of Fluids and Structures*.

Murua, J., Palacios, R. and Graham, J.M.R., 2012. "Applications of the unsteady vortex-lattice method in aircraft aeroelasticity and flight dynamics". *Progress in Aerospace Sciences*.

Palacios, R., Murua, J. and Cook, R., 2010. "Structural and aerodynamic models in nonlinear flight dynamics of very flexible aircraft". *AIAA Journal*.

Petot, D., 1983. "Progress in the semi-empirical prediction of the aerodynamic forces due to large amplitude oscillations of an airfoil in attached or separated flow". *Tech. Rep. 1983-111*.

Ramesh, K., Gopalarathnam, A., Edwards, J.R. and et al., 2013. "An unsteady airfoil theory applied to pitching motions validated against experiment and computation". *Theoretical and Computational Fluid Dynamics*, Vol. 27(6).

Ramesh, K., Gopalarathnam, A., Granlund, K. and et al., 2014. "Discrete-vortex method with novel shedding criterion for unsteady airfoil flows with intermittent leading-edge vortex shedding". *Journal of Fluid Mechanics*, Vol. 751.

Ramesh, K., Gopalarathnamand, A., Ol, M.V. and et al, 2011. "Augmentation of inviscid airfoil theory to predict and model 2d unsteady vortex dominated flows". *AIAA Paper*.

Ramesh, K., Monteiro, T.P., Silvestre, F. and et al, 2017. "Experimental and numerical investigation of post-flutter limit cycle oscillations on a cantilevered flat plate". *IFASD*.

Ramesh, K., Murua, J. and Gopalarathnam, A., 2015. "Limit-cycle oscillations in unsteady flows dominated by intermittent leading-edge vortex shedding". *Journal of Fluids and Structures*, Vol. 55.

Shearer, C.M. and Cesnik, C.E.S., 2007. "Nonlinear flight dynamics of very flexible aircraft". *Journal of Aircraft*.

Shyy, W. and Liu, H., 2007. "Flapping wings and aerodynamic lift: The role of leading-edge vortices". *AIAA Journal*, Vol. 45(12).

Silvestre, F.J. and Luckner, R., 2015. "Experimental validation of a flight simulation model for slightly flexible aircraft". *AIAA Journal*.

Silvestre, F.J., Neto, A.B.G., Bertolin, R.M. and et al., 2016. "Aircraft control based on flexible aircraft dynamics". *Journal of Aircraft*.

Spalart, P. and Allmaras, S., 1992. "A one-equation turbulence model for aerodynamic flows". *30th Aerospace Sciences Meeting and Exhibit, American Institute of Aeronautics and Astronautics*.

SureshBabu, A., Ramesh, K. and Gopalarathnam, A., 2019. "Model reduction in discrete-vortex methods for unsteady airfoil flows". *AIAA Journal*.

Tang, D.M., Yamamoto, H. and Dowell, E.H., 2003. "Flutter and limit cycle oscillations of two-dimensional panels in three-dimensional axial flow". *Journal of Fluids and Structures*, Vol. 17(2).

Theodorsen, T., 1935. "General theory of aerodynamic instability and the mechanism of flutter". NACA Rept. 496.

Theodorsen, T. and Garrick, I.E., 1942. "Flutter calculations in three degrees of freedom". NACA Rept. 741.

Vatistas, G.H., Kozel, V. and Mih, W.C., 1991. "A simpler model for concentrated vortices". *Experiments in Fluids*, Vol. 11(1).

von Kármán, T. and Burgers, J.M., 1963. "General aerodynamic theory - perfect fluids". *Aerodynamic theory: a general review of progress*.

Wagner, H., 1925. "Über die entstehung des dynamischen auftriebes von tragflügeln". ZaMM.

Wang, C. and Eldredge, J.D., 2012. "Low-order phenomenological modeling of leading-edge vortex formation". *Theoretical and Computational Fluid Dynamics*, Vol. 27(5).

Yoshikazu, H., 2016. *Leading-Edge-Vortex Formation on Finite Wings in Unsteady Flow*. Ph.D. thesis, North Carolina State University.

Yoshikazu, H., Minao, S., Ashok, G. and Edwards, J.R., 2021. "Flow criticality governs leading-edge-vortex initiation on finite wings in unsteady flow". *J. Fluid Mech*.

9. RESPONSIBILITY NOTICE

The authors are solely responsible for the printed material included in this paper.